Hao FU · Chuangxin HE · Yingzheng LIU

Flow structures of a precessing jet in an axisymmetric chamber

Abstract This work investigates the flow structures of a precessing jet in an axisymmetric chamber with expansion ratio $D/d = 5$ and length-to-diameter ratio $L/D = 2.75$ at Reynolds number $\mathrm{Re}_d = 2.4 \times 10^4$ by use of planar particle image velocimetry. Time-averaged and statistical results indicate that the precessing jet flow is symmetric, on average, in the streamwise plane. Large velocity fluctuations and vorticity exist in the inner and outer shear layers. In addition, vorticity is found in the boundary layer of the chamber wall, due to backflow and confinement. Subsequent correlative analysis indicates that coherent structures are mainly distributed in the shear layer and decay with its development. The results also indicate that precession occurs in the region $x/d > 5$ and may lead to changes in the structure and position of the shear layer. Further spectral analysis shows that a low-frequency structure with St $\approx 7.4 \times 10^{-3}$, which can be interpreted as precession, exists in the flow field and that the corresponding dominant frequency decreases as the fluid flows downstream. Finally, proper orthogonal decomposition (POD) analysis reveals the most energetic mode representing the flow structure of precession, which has the highest proportion of the total downstream energy. The precession induces an alternating flow, switching between outflow from one side of the chamber and inflow from another side. In addition, four typical instances of flow structures of precession with different intensities or phases are presented through low-order reconstruction of the specified POD modes. These cases show that due to the instability of the reattachment point, the mainstream oscillates up and down in the region near the nozzle exit and twists back and forth in the region near the chamber exit, with changes of scale and position of flow structures on the measurement plane, exposing complex behavior of the instantaneous flow field of precession.

Keywords Flow structures · Precessing jet · POD

1 Introduction

Precessing jet flows, which are formed by issuing a round jet into an axisymmetric chamber with large expansion, have found widespread use in various combustors (Kandakure et al. 2008) for their excellence in mixing fuels and in improving flame stability (Newbold et al. 2000). In such a configuration, the jet flow asymmetrically attaches to the chamber wall while azimuthally precessing about the chamber axis; this is closely related to flow instabilities during sudden expansions of axisymmetric chambers. There is no doubt

H. FU · C. HE (✉) · Y. LIU
Key Lab of Education Ministry for Power Machinery and Engineering, School of Mechanical Engineering, Shanghai Jiao Tong University, 800 Dongchuan Road, Shanghai 200240, China
E-mail: chuangxin.he@sjtu.edu.cn

H. FU · C. HE · Y. LIU
Gas Turbine Research Institute, Shanghai Jiao Tong University, 800 Dongchuan Road, Shanghai 200240, China

that unsteady behaviors of the jet flow are overwhelmingly dominated by its large-scale azimuthal precession (Newbold et al. 2010), while superimposed flow structures can introduce considerable complexity. Accordingly, an insightful understanding of flow structures of the precessing jet is highly desirable.

Much research has been undertaken to determine the characteristics of precessing jets in an axisymmetric chamber. Jet precession was first identified by Nathan (1988) using flow visualization techniques. His results showed that a reattaching jet moved azimuthally around the wall of its chamber and that a recirculating flow region was formed opposite to the location of the jet in the flow. For flow at Reynolds number Re_d ($Re_d = ud/v > 2.0 \times 10^4$) in an axisymmetric chamber with expansion ratio $D/d = 5.16$ between the chamber and nozzle diameters, Nobes (1997) used Mie scattering to determine the mixture field of a passive conserved scalar, confirming that large-scale and long-lived features exist in the external flow of a precessing jet. Subsequent studies by Newbold (1998) indicated that precession occurs over the range $2 \leq L/D \leq 3.5$ for $D/d = 5$ when $Re_d > 1.0 \times 10^4$, where L is the chamber length. Detailed measurements of precessing jet flow at $5.3 \times 10^4 < Re_d < 13.4 \times 10^4$, $D/d = 6.4$ and $L/D = 2.6$ were conducted by Nathan et al. (1998). Their results showed that the bistable flow intermittently and chaotically switches between the precessing jet (PJ) mode and the axial jet (AJ) mode, where the jet exiting the nozzle/chamber closely resembles an axisymmetric jet. The Strouhal number of the precession, $St = fd/u$, was measured using pressure transducers and found to be almost independent of Re_d for $Re_d > 2.0 \times 10^4$. Consistently, Wong et al. (2008) claimed that detailed measurements made under fixed conditions could be considered to be broadly representative of precessing jet flow through the chamber. For flow at $Re_d = 8.45 \times 10^4$ with $D/d = 5.07$, $L/D = 2.7$, Wong et al. (2003) determined the internal flow field using phase-averaged laser Doppler measurements and found that the internal velocity field decays more rapidly in the PJ mode than in the AJ mode. The asymmetric deflection of the jet and its reattachment to the chamber wall were clearly observed. Furthermore, for flow at $Re_d = 3.0 \times 10^4 \sim 9.0 \times 10^4$, Wong et al. (2008) used planar particle image velocimetry (PIV) to examine the flow field immediately beyond the chamber. Their results indicated that the jet emerging from the nozzle departs with an azimuthal component in the direction opposite to that of the jet precession. Later, a tomographic PIV measurement of the precessing jet flow (Cafiero et al. 2014) at $Re_d = 15 \times 10^4$ ($D/d = 5$, $L/D = 2.75$) identified two helical structures embedded within the jet near the inlet plane, which correspond to a swirling motion. For the same flow configuration ($Re_d = 4.25 \times 10^4$), Ceglia et al. (2017) showed that the entrainment process influences the instantaneous organization of the large-scale coherent structures during precession. However, to the best of the authors' knowledge, very limited research (Ceglia et al. 2017; Chen et al. 2017; Wong et al. 2008, 2003) has been conducted to determine the dynamics of flow structures superimposed on a precessing jet.

This experimental study focuses on the flow structures of a precessing jet in an axisymmetric chamber. The expansion ratio D/d and chamber length-to-diameter ratio L/D are 5 and 2.75, respectively, the optimal dimensions to generate precession (Nathan et al. 1998). The Reynolds number (Re_d), based on the nozzle diameter and bulk velocity U_0 in the tube upstream of the nozzle, is 2.4×10^4. The velocity fields near the nozzle exit (zone I) and chamber exit (zone II) are measured separately using planar PIV. Spectral analysis and the $v'-v'$ correlation coefficient are used to determine quasiperiodic and spatial characteristics of large-scale structures. Finally, proper orthogonal decomposition (POD) analysis is used to delineate large-scale flow structures and a POD reconstruction is made to aid understanding of the instantaneous flow fields.

2 Experimental setup

The experiment was performed in a glass tank measuring 3000 mm (length) $\times$ 550 mm (width) $\times$ 700 mm (depth), as shown in Fig. 1a. The glass tank was filled with tap water, which was filtered by a 5 μm filter to ensure quality, to ensure that the water level far exceeded the top of the chamber. The flow was supplied from a submersible pump mounted at the bottom of the tank. A transformer, connected to the pump, was used to control the flow velocity. The water flowed from the pump to a large cylindrical settling chamber, in which were placed a honeycomb, wire mesh and a glass plate with many small holes to improve flow quality. It then flowed through a supply pipe and a nozzle with 0° straight blades into an axisymmetric chamber. All of the above flow passage devices were mounted to ensure that their centers had the same height. Figure 1b shows some important geometric sizes for a precessing jet flow in an axisymmetric chamber. The inner diameter (d) of the nozzle used here was 40 mm, the same as by He et al. (2019). The length (L) and inner diameter (D) of the axisymmetric chamber were 550 mm and 200 mm, respectively, yielding expansion ratio $D/d = 5$ and chamber length-to-diameter ratio $L/D = 2.75$. The transformer was

held at a constant position during the experiment, yielding $Re_d = 2.4 \times 10^4$ based on d and bulk velocity U_0 in the supply pipe.

The flow field in the streamwise (x–y) plane was measured by planar PIV, as shown in Fig. 1a. The tank was seeded with glass beads ($\rho \approx 1.05$ kg/m^3, $d_I \approx 10$ μm). Illumination was provided by a 5-W continuous-wave semiconductor laser, with sheet optics configured to produce 1-mm-thick laser (532 nm wavelength) sheets on the measurement plane. During the experiment, the laser was placed in modulation mode, supporting its use as a pulse laser. A high-pixel-density CCD (4872 × 3248 pixels) camera (IPX 16 M, IMPERX, USA) was used to capture the seeded flow patterns. The camera and laser were connected with a synchronizer to ensure accurate timing. The region of interest for the PIV measurement extended from the nozzle exit to the region near the chamber exit. However, the velocity fields in zone I and zone II were measured separately due to the limitation in laser intensity. The ranges of measurement in the streamwise direction were $0 \sim 7d$ and $5 \sim 14d$, respectively, yielding overlap area $2d$, which aimed to obtain statistical results of the full field by combining two regions. In the experiment, a total of 4000 images (2000 per zone) of the seeded flow were successively recorded by the camera at a frequency of 1 Hz. The standard PIV cross-correlation algorithm, incorporating window offset, sub-pixel recognition and distortion correction, was used to determine accurate velocity fields. The interrogation window size was 32 × 32 pixels with a 50% overlap, yielding a measurement grid of velocity vectors with a spacing of 1.4 × 1.4 mm. The measurement error for particle displacement between two images was less than 0.1 pixels, and the uncertainty in the PIV measurement of the velocity field was smaller than 2%.

3 Results and discussion

3.1 Time-averaged and statistical characteristics

A preliminary view of the flow characteristics of a precessing jet in an axisymmetric chamber was obtained by plotting a time-averaged streamline pattern, as shown in Fig. 2. The statistical results in zone I and zone II were calculated individually and combined to give the full field. The results in the overlapping region were constructed using a weighted average of the two to carefully match the fields in each zone. The full field is symmetric in the streamwise plane, which is in good agreement with the study conducted by Nathan et al. (1998). The fluid ejects from the nozzle and forms two large-scale vortex structures in opposing directions, symmetrically distributed on both sides of the axis due to confinement by the chamber wall. The vortex center, determined using the Γ_1-criterion (Graftieaux et al. 2001), is located about $7.5d$ from the nozzle in the streamwise direction and $1.5d$ vertically from the axis. In addition, the inner and outer boundaries of the shear layer can be seen intuitively with the inner boundaries meeting approximately at $x/d = 5$, resulting in the end of the potential core. However, the outer boundaries spread outward to a certain extent and then shrink slightly until the far field is reached, likely caused by chamber wall confinement. There is a region of relatively low-velocity recirculation in the center of the nozzle exit, due to the boundary effects of the vanes and hub (He et al. 2019).

To further evaluate the intensified flow fluctuations, a contour plot of the root mean square (RMS) streamwise velocity fluctuation intensity, normalized by bulk supply pipe velocity, is shown in Fig. 3. High-streamwise-velocity fluctuations appear in the upper and lower shear layers ($y/d = \pm 0.5$) near the nozzle exit, with a maximum value close to 0.7, and decrease gradually in the streamwise direction. Consulting the literature (Ball et al. 2012), this can be interpreted as the presence of large-scale coherent structures in the initial regions of the shear layers, which decay with the development of the flow. The high region appearing around $y/d = \pm 0.15$ and the low region at the center, near the nozzle exit, are associated with the inner shear layer caused by the hub. The outer and inner shear layers can be seen intuitively in Fig. 4, which shows the time-averaged vorticity field. Vorticity mainly occurs in the inner and outer shear layers and decays as these layers develop, which demonstrates that the shear layer vortices initiate at the nozzle exit, expanding in size as the fluid flows downstream (He and Liu 2017). In addition, vorticity is found near the chamber wall, the recirculation region shown in Fig. 2. This may be interpreted as the phenomenon of fluid outside the chamber flowing into the chamber along its wall, resulting in vortex generation in the boundary layer of the wall.
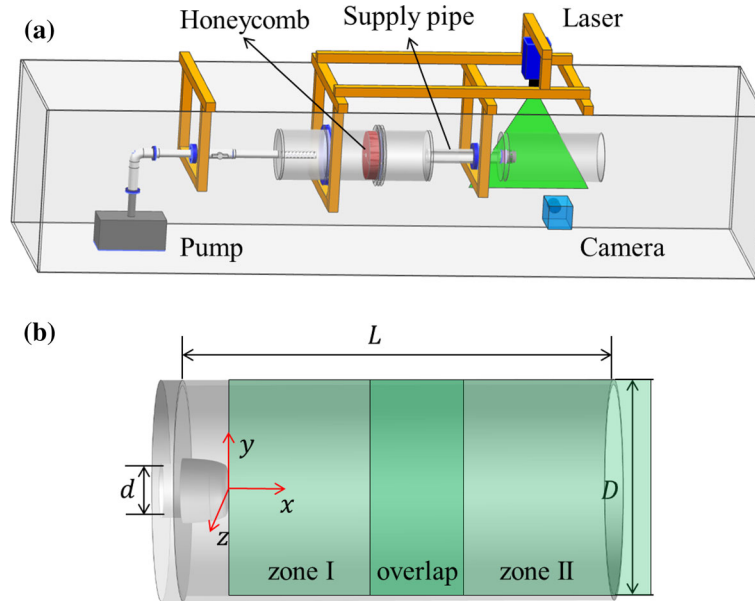
Fig. 1 Schematic diagram of the experimental setup and (b) some important geometric sizes

3.2 Correlative and spectral analysis

To characterize the large-scale structures and organization of a precessing jet in an axisymmetric chamber, the two-point spatial correlation coefficients of the vertical velocity fluctuations were calculated as:

$$R_{v'v'} = \frac{\langle v'(x,y)v'(x_0, y_0)\rangle}{\langle v'_{\mathrm{rms}}(x,y)v'_{\mathrm{rms}}(x_0, y_0)\rangle} \tag{1}$$

where x_0 and y_0 represent the reference points, which are shown in Fig. 4. Six reference points, $x_0/d = 1 \sim 11$ (in increments of 2) and $y_0/d = -0.5$, were selected according to the above analysis for examining the large-scale structures buried in the outer shear layer. Figure 5 shows a contour plot of the spatial v'–v' correlation coefficients at various reference points. The correlation contours that lie between -0.1 and 0.2 are blanked, to better illustrate the distinct variance in the jet flow dynamics at different reference points. The increase in size of correlation structures in the downstream direction indicates the extent of growth in their length scale, which is associated with organized motion in the jet flow. At the reference points near the nozzle exit ($x_0/d = 1$ and 3), a highly concentrated positive correlation zone is centered at the reference position and a small negative correlation zone exists on each side. Meanwhile, the correlation zones do not develop horizontally along the streamwise direction, but rather incline toward the axis. This indicates a periodic rollup of the shear layer and a tendency of the inner boundaries to meet. However, when the reference point moves to $x_0/d = 5$, the upstream negative correlation zone disappears and its downstream counterpart becomes chaotic. Similarly, when the reference point moves further downstream to $x_0/d = 7$ and 9, no concentrated negative correlation zone is detected on either side. This indicates that the structure and development of the shear layer are different from those in the axisymmetric jet without precession (Crow and Champagne 1970; Yule 1978) from $x/d > 5$. It can be further inferred that precession occurs and induces a change in the shear layer development in this region. These results are consistent with those in the literature (Hill et al. 1995). However, the negative correlation zone downstream reappears, with a larger area, at reference point ($x_0/d = 11$) near the chamber exit, which indicates that flow in the far field is more akin to an axisymmetric jet without precession. This result is in good agreement with studies by Newbold (1998) and Parham et al. (2005).

To obtain further evidence of the existence of precession and its spectral signature in the flow field, the spectral characteristics of the flow were analyzed. Because the jet was known to attach to the chamber wall when precession occurs, points near to the wall were selected ($y/d = 2$) to determine whether precession occurs. Figure 6a, b shows the power spectral density (PSD) of streamwise velocity at different points in zone I and zone II, respectively. The selection of points in the streamwise direction was aimed to determine
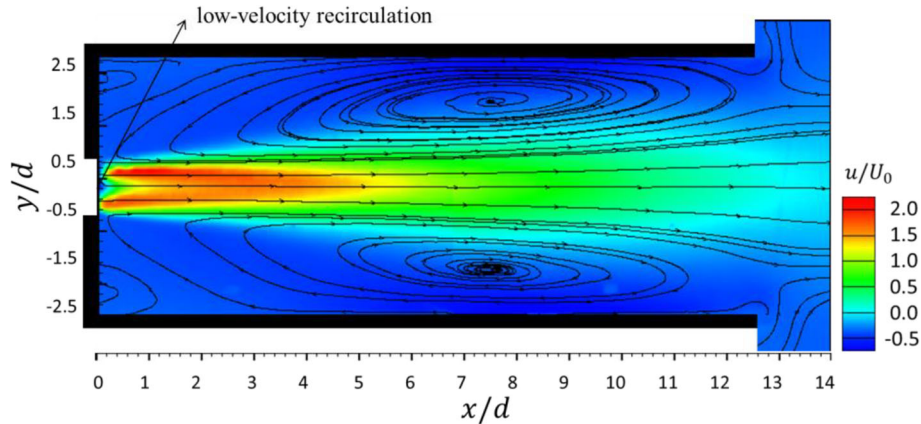
**Fig. 2** Streamline pattern and contour plot of time-averaged streamwise velocity

the region affected by precession and to study the developmental characteristics of the precession. The PSD at different points in zone I had good consistency, as shown in Fig. 6a, which means that the regions containing these points fell within the same flow structures. A peak with Strouhal number $St = fd/U_0 \approx 7.4 \times 10^{-3}$ indicated the existence of a low-frequency periodic structure in the flow-field. Comparing with results in the literature (Mi and Nathan 2004; Mi et al. 2006), it could be concluded that this low-frequency structure was precession. This precession was also found in zone II at a lower frequency with $St \approx 6.0 \times 10^{-3}$, as shown in Fig. 6b. The dominant frequency decreased with distance downstream, in good agreement with the study by Zaouali et al. (2013).

3.3 POD analysis

To determine the large-scale flow structures relevant to a precessing jet in an axisymmetric chamber, a POD analysis on the velocity field was conducted. The POD analysis, which was designed to find the optimal representation of field realizations by extracting the most energetic eigenmodes of fluctuation, was implemented using the snapshot method (Sirovich 1987a, 1987b, 1987c). Detailed information regarding this method, including fundamentals and mathematical procedures, has been reported in studies by Hutchinson (1971). By conducting a POD analysis on the flow database of a precessing jet in an axisymmetric chamber independently in each zone, the POD modes indicating the spatial features of the dominant flow structures, the mode coefficients containing temporal evolution information, as well as the eigenvalues reflecting the relative contributions to the total turbulent kinetic energy (TKE) of the fluctuating velocity field can be successfully extracted (Wang et al. 2018). Therefore, the dominant flow structures of a precessing jet in an axisymmetric chamber can be identified by ranking the POD modes by their energy
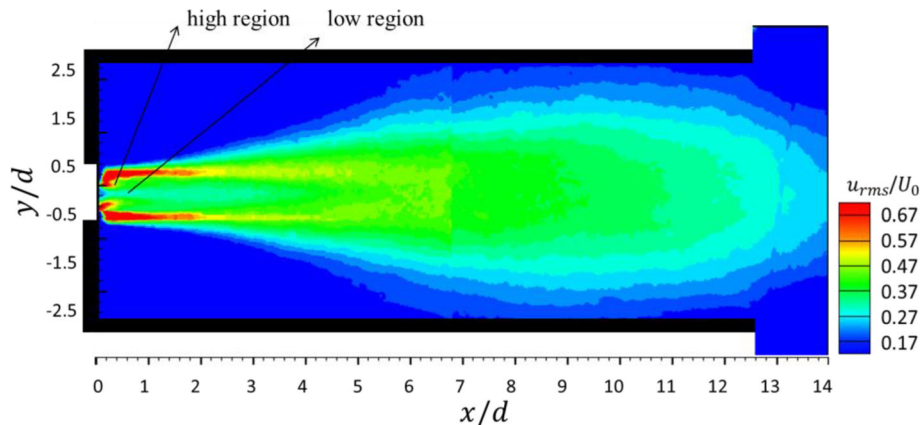
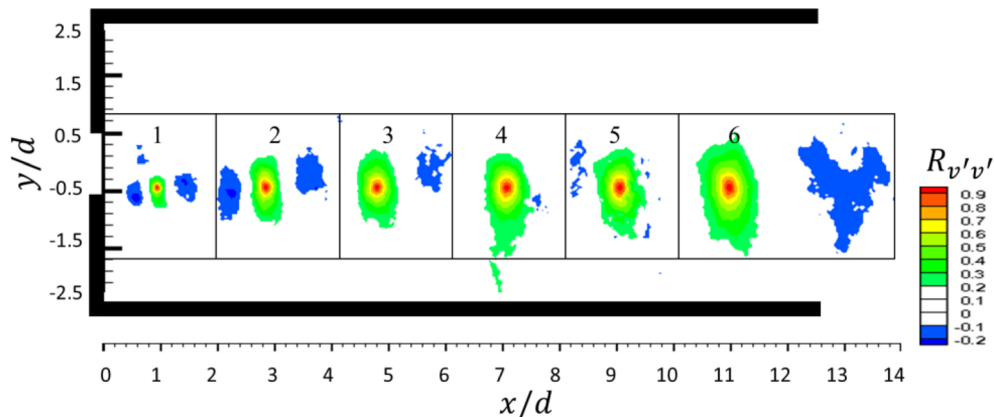**Fig. 3** Contour plot of streamwise velocity fluctuation intensity
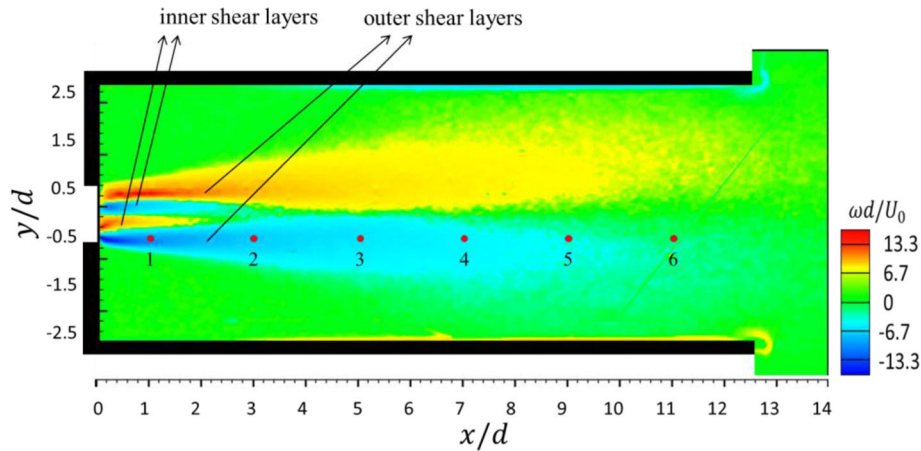
**Fig. 4** Contour plot of time-averaged vorticity

contributions, while the spatial distribution and time evolution of the flow structures are, respectively, determined by their mode distributions and mode coefficients.

Figure 7 displays the profiles of the eigenvalue with respect to the first 10 POD modes in each zone. The magnitude of the eigenvalue reflects the relative contribution of the eigenmode to the total TKE. For the flow in both zones, a global view of the two curves shows that the eigenvalue rapidly decreases as the POD mode increases up to eight. Mode 1 is the major contributor (11.5 and 13.5%, respectively) to the total fluctuating energy in zone I and zone II, due to the overwhelming dominance of flow structures in mode 1. A drastic reduction in the fluctuation energy is observed from the first to the second mode (4.2 and 6.6%), further emphasizing the dominance of the large-scale structures contained in the first mode in each zone. In addition, the fluctuation energy of each mode in zone II is slightly larger than that of the same mode in zone I, indicating that the dominance of the unsteady events is enhanced in the downstream region.

To reveal the spatial features of the flow structures of a precessing jet in an axisymmetric chamber, the vectorized streamwise velocity components of the first 8 POD modes and the corresponding PSD spectra of the mode coefficients in zone I and zone II are shown in Figs. 8 and 9, respectively. Here, each mode is normalized by its norm and each spectrum is normalized by its maximum value in the St range of view. Mode 1 exhibits two large regions with significant velocity fluctuations, which are symmetrically distributed to the sides of the axis, occupying almost half of zone I as shown in Fig. 8a. In addition, the region with significant positive velocity fluctuations in the upper half of the chamber indicates that the flow proceeds directly downstream from there. However, the region with significant negative velocity fluctuations in the lower half of the chamber indicates backflow. Meanwhile, the PSD spectrum of the mode 1 coefficient is shown in Fig. 9a. An obvious peak with $St \approx 7.4 \times 10^{-3}$, which is the same frequency as the PSD of the streamwise velocity, demonstrates that large-scale structures in mode 1 are the flow structures of precession.


Fig. 5 Contour plot of spatial correlation coefficient in reference to: $x0/d = 1 \sim 11$ with increments of 2, $y0/d = -0.5$
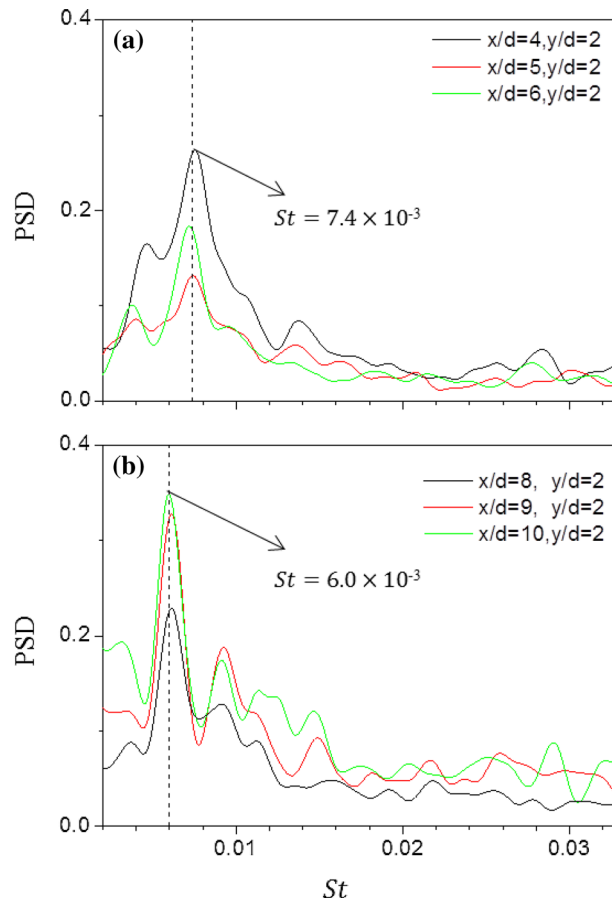
Fig. 6 Power spectral density of streamwise velocity at different locations: **a** zone I; **b** zone II

There is also an obvious peak with $St \approx 7.4 \times 10^{-3}$ in the PSD spectrum of modes 3 and 5 as shown in Fig. 9c and e, which suggests that the flow structures in these modes may be associated with precession. For mode 3, a counterclockwise vortex appears at the axle center upstream of the regions with significant velocity fluctuations, as shown in Fig. 8c. Another counterclockwise vortex appears on each side, near these regions. Furthermore, the areas of regions with significant velocity fluctuation decrease. However, for mode 5, two regions with significant velocity fluctuation and two vortices near those regions move upstream and have opposite direction, with positive becoming negative and counterclockwise becoming clockwise as shown in Fig. 8e. These two modes represent the small-scale structures near the initial position of precession. For mode 2, the flow is almost backflow in the whole space, as shown in Fig. 8b, and has a very low frequency with $St < 1.0 \times 10^{-3}$, as shown in Fig. 9b. This phenomenon can be associated with the recirculation flow caused by confinement. For mode 4, the flow is similar to an axisymmetric jet colliding with the backflow caused by precession, as shown in Fig. 8d. The flow structures of the AJ mode dominate the flow field, so there is no dominant frequency in Fig. 9d. Modes 6–8 are shown in Fig. 8f, g, h; their PSD spectra have many peaks due to a broad range of eddy frequencies prevailing in the turbulent precessing jet flow in an axisymmetric chamber, as shown in Fig. 9f-h. However, it is not possible to associate them with a specific physical mechanism. Modes 7 and 8 are characterized by smaller-scale structures in the shear layer with higher frequencies, which can be inferred to be related to the shear layer structures (Semeraro et al. 2012).

The vectorized streamwise velocity components of the first 8 POD modes and the corresponding PSD spectra of the mode coefficients in zone II are shown in Figs. 10 and 11, respectively. In Fig. 10a, mode 1 exhibits similar flow structures to those in zone I: two large regions with significant velocity fluctuations. The PSD spectrum of the mode 1 coefficient is shown in Fig. 11a. An obvious peak with $St \approx 6.0 \times 10^{-3}$, which is the same frequency as the PSD of the streamwise velocity, demonstrates that the large-scale structures in mode 1 are the flow structures of precession, just like in zone I. However, distinct from zone I,
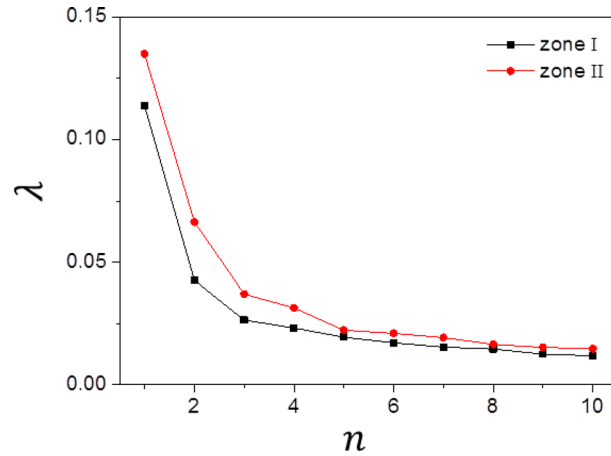
**Fig. 7** Normalized eigenvalues of the first 10 POD modes

no other modes can be proved to be highly associated with precession from the PSD spectrum in Fig. 11b, c, d, e, f, g, h, as there is no dominant frequency with St $\approx 6.0 \times 10^{-3}$. In addition, the flow in mode 2 is a typical AJ mode without dominant frequency, as shown in Figs. 10b and 11b. There is a region with significant positive velocity fluctuation at the center downstream, which indicates the obvious streamwise oscillation in the far field. For mode 3 in Fig. 10c, the flow is very similar to precession: The fluid flows out close to the wall of the chamber, causing the environmental fluid to flow in from the middle of the chamber exit. However, the precession has a larger scale, just as for mode 1, because the POD mode is composed of flow structures at multiple frequencies and precession may have no obvious advantage in this mode, for there is no dominant frequency with St $\approx 6.0 \times 10^{-3}$, as shown in Fig. 11c. In addition, a strong similarity between modes 4 and 6 can be observed in Fig. 10d, f. The appearance of POD modes in pairs is common when the buried coherent structures are convective (Kiya and Sasaki 1983). Essentially, both modes in a pair represent the same structure, but with a spatial shift in the streamwise direction (Zhang and Liu 2015). In the fourth POD mode, clockwise and counterclockwise structures are found at the center of stations $x/d = 8$ and 12.5, respectively; clockwise, counterclockwise and clockwise structures are found at the center of the stations $x/d = 7$, 10.5 and 14, respectively. Thus, the pair of coupled POD modes gives a representation of the large-scale vortical structures buried in the shear layer, which are related to the large-scale (flapping) oscillation of the inner jet (Semeraro et al. 2012). However, it is difficult for higher-order modes to be effectively described by a frequency spectrum due to the superposition of multiple oscillation frequencies, as shown in Fig. 11d, f. The remaining three modes in Fig. 10e, g and h are more difficult to associate with a physical mechanism for the same reason and are not discussed further.

3.4 POD reconstruction

The flow field contains vortex structures of various scales. It is difficult to visually observe the spatial distribution characteristics of large-scale coherent structures in the flow field due to the influence of various small-scale vortex structures and turbulence dissipation on the flow field. Through POD analysis, it is understood that low-order POD modes represent large-scale coherent structures with a high energy proportion, while high-order POD modes represent small-scale structures with a low energy proportion and background noise. For this reason, we choose to reconstruct the flow field to filter small-scale structures and background noise, so as to observe the spatial distribution characteristics specifically of large-scale coherent structures. The low-order modes whose total energy proportion exceeds 90% of the total TKE are used as the truncation order for POD reconstruction, and none of the remaining modes has more than a 1% energy proportion (Deane and Sirovich 1991).

The first POD mode represents the flow structure of precession, and therefore reveals the time evolution of this flow structure. Figure 12 shows the temporal variation of the first POD mode coefficient in zone I. There are two typical regions of amplitude, indicating that two typical flow structures of precession with differing intensities exist. Meanwhile, the positive and negative values of amplitude also indicate phase information. To characterize the large-scale coherent structures and global variation of precession, four typical instants are chosen as shown in Fig. 12 and the corresponding streamline pattern and contour plot of
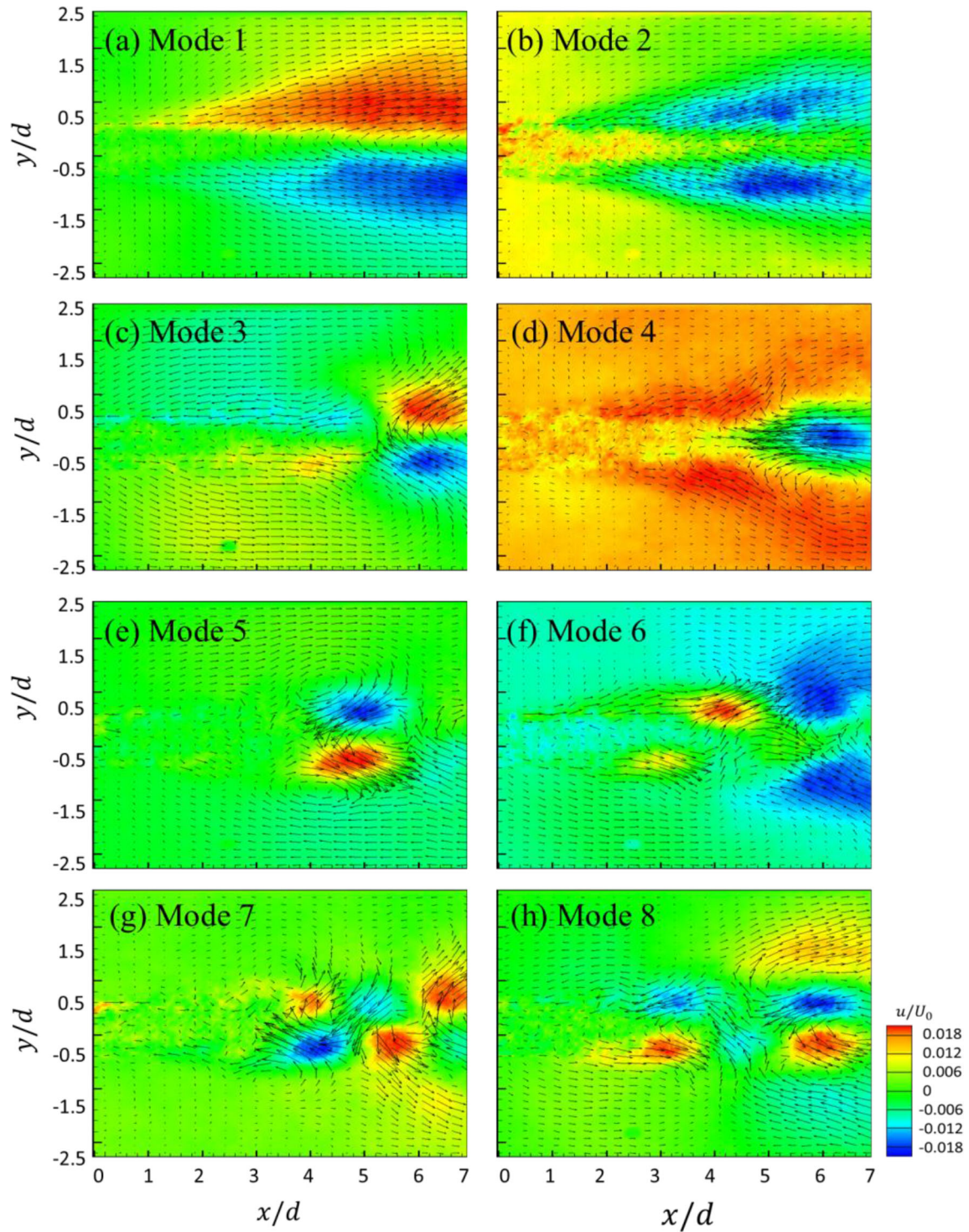
Fig. 8 First 8 POD modes in zone I

the streamwise velocity field in zone I are shown in Fig. 13. Instants T_1 and T_3 represent the moment when precession has just begun or has low intensity, while instants T_2 and T_4 represent the moment when precession is strongest. A global view of the four typical instants is analogous to the self-sustained oscillation flow in a double-cavity channel (Fu et al. 2020). The mainstream swings up and down in the measuring plane, as precession causes the mainstream to reattach to the chamber wall, but the reattachment
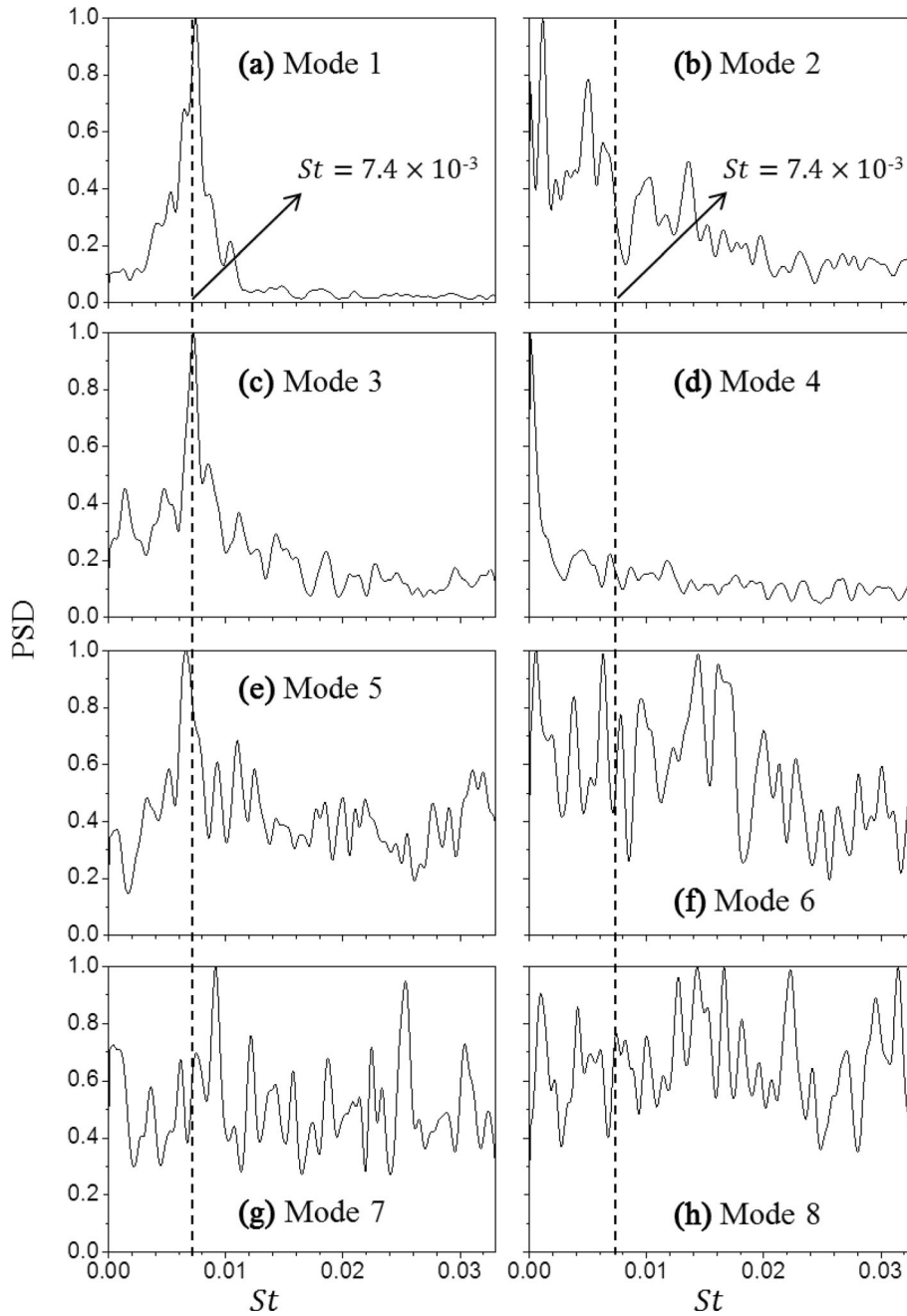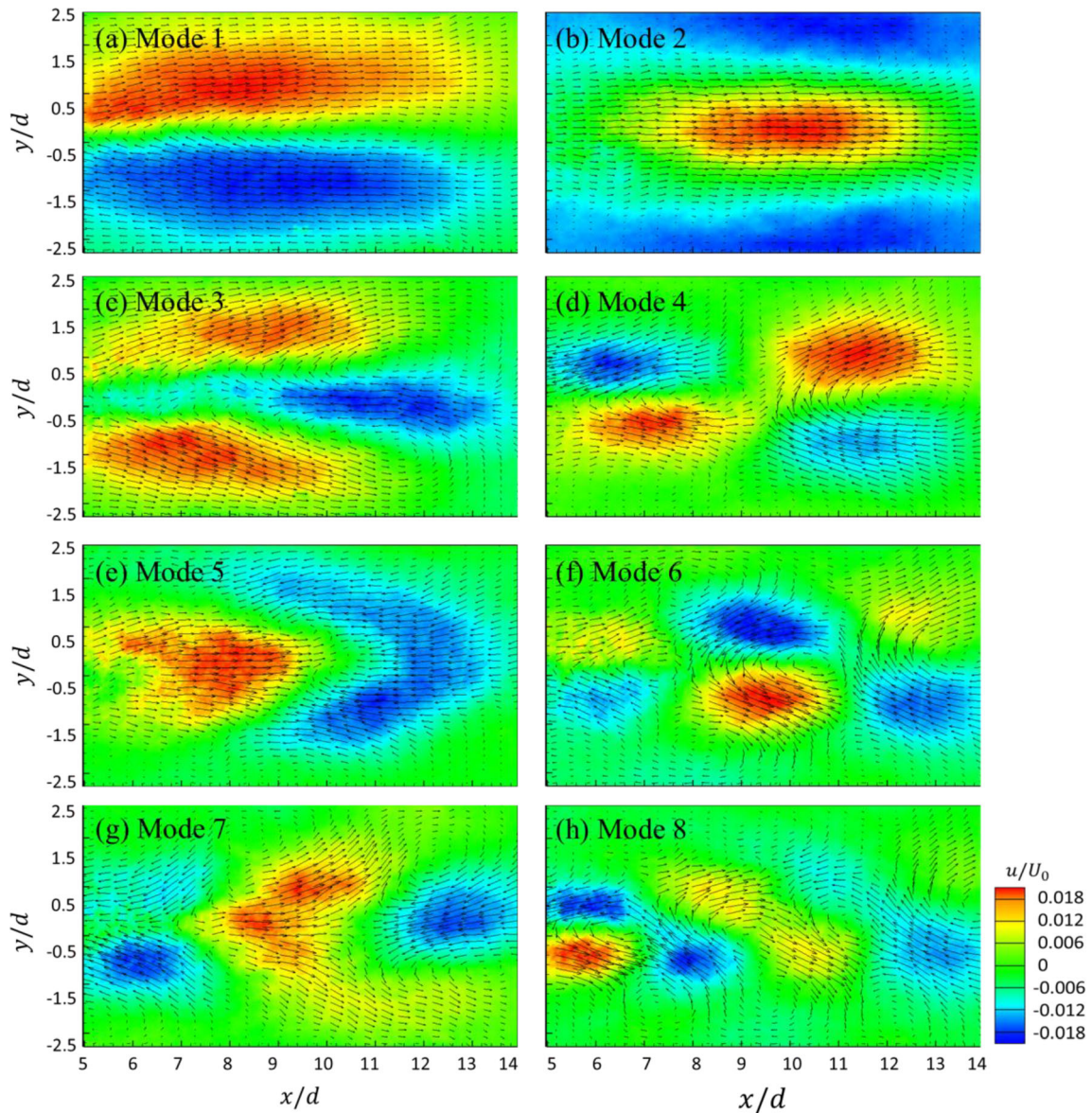
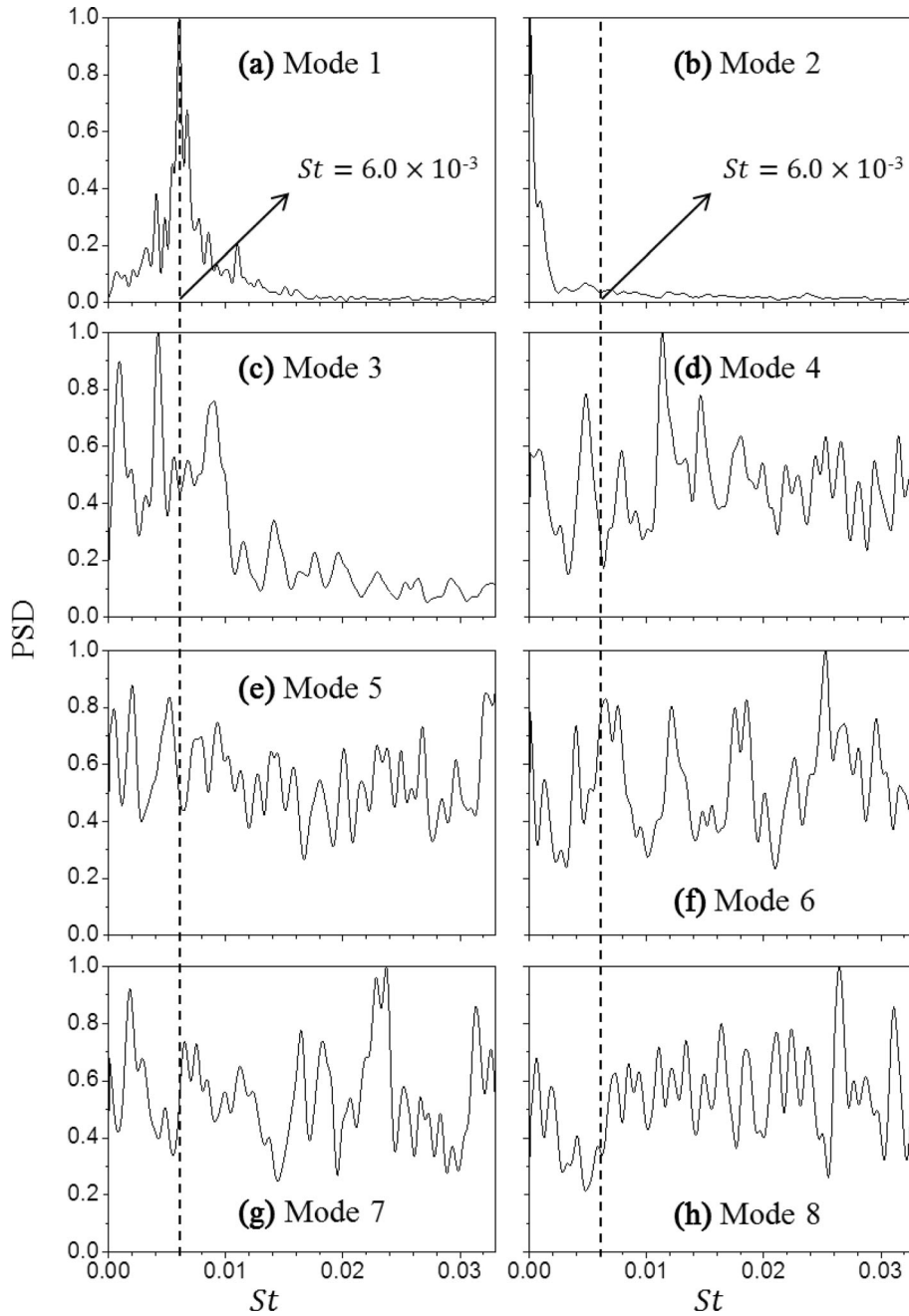**Fig. 9** Power spectral density of the POD mode coefficients in zone I

point is unstable and then moves azimuthally. However, further detailed observation indicates that there are many small-scale structures on both sides of the mainstream and that their distribution is not symmetrical along the axis at instant T_1, as shown in Fig. 13a. Meanwhile, the tendency of the mainstream to bend to one side is not obvious at this moment. At instant T_2, the mainstream bends further toward the top of the chamber due to the stronger intensity of precession, as shown in Fig. 13b. The location where the mainstream starts to bend is approximately $x/d = 4 \sim 5$, indicating that precession occurs from this region, in good agreement with the correlative analysis above. In addition, some relatively large structures appear upstream of the bending side of the mainstream, while some small structures move up with the mainstream. Figure 13c, d exhibits the chosen two typical instants when the mainstream bends downward, with different precession intensities. At instant T_3, the downward bending of the mainstream has occurred at

approximately $x/d = 6$, with some relatively large structures also appearing upstream of the bending side of the mainstream. In addition, the mainstream bends further at instant T_4.

The temporal variation of the first POD mode coefficient and the chosen four typical instants in zone II is shown in Fig. 14, with the corresponding streamline pattern and contour plot of streamwise velocity field in zone II shown in Fig. 15. As compared to zone I, the mainstream is no longer swinging up and down, but rather twisting forward. This may be due to a stronger oscillation of the jet in the far field. At instant T_1, the mainstream does not bend upward to the wall, but begins to bend downward at the position of $x/d = 8$ and then bends upward again at $x/d = 10.5$ until it flows out of the chamber, as shown in Fig. 15a. In addition, some complex structures appear at the place where the bending direction changes. However, when the precession is stronger at instant T_2, as shown in Fig. 15b, the mainstream bends upward until $x/d = 10.5$ and then bends down slightly. In addition, the area of the recirculation region under the mainstream is larger. Instants T_3 and T_4 exhibit similar results to instants T_1 and T_2, although they include more small structures on the opposite of the mainstream bends, as shown in Fig. 15c. In addition, more complicated structures exist near the reattached chamber wall due to the twisting of the mainstream shown in Fig. 15d.


**Fig.10** First 8 POD modes in zone II

Fig.11 Power spectral density of the POD mode coefficients in zone II

4 Conclusions

In this study, the flow structures of a precessing jet in an axisymmetric chamber with expansion ratio $D/d = 5$ and length-to-diameter ratio $L/D = 2.75$ were comprehensively experimentally investigated. In the experiment, the Reynolds number was maintained at 2.4×10^4 and the flow fields of the region near the nozzle exit (zone I) and near the chamber exit (zone II) with overlap area $2d$ in the streamwise direction were obtained separately by planar PIV. Time-averaged and statistical results of the full field were obtained by combining the two zones and indicated that a precessing jet flow was symmetric, on average, in the streamwise plane. The results in the overlapping region were constructed using a weighted average of the two to carefully match the fields in each zone. Large velocity fluctuations and vorticity appeared in the inner
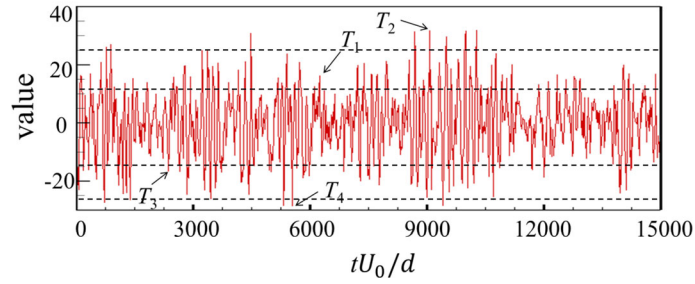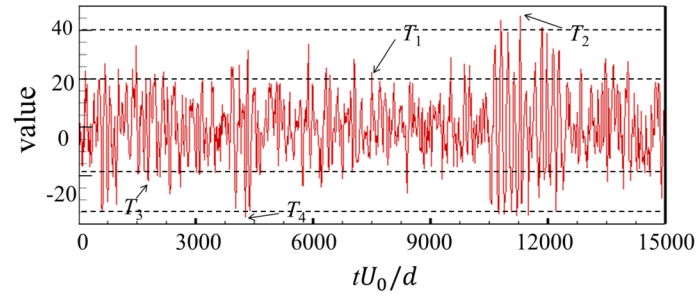
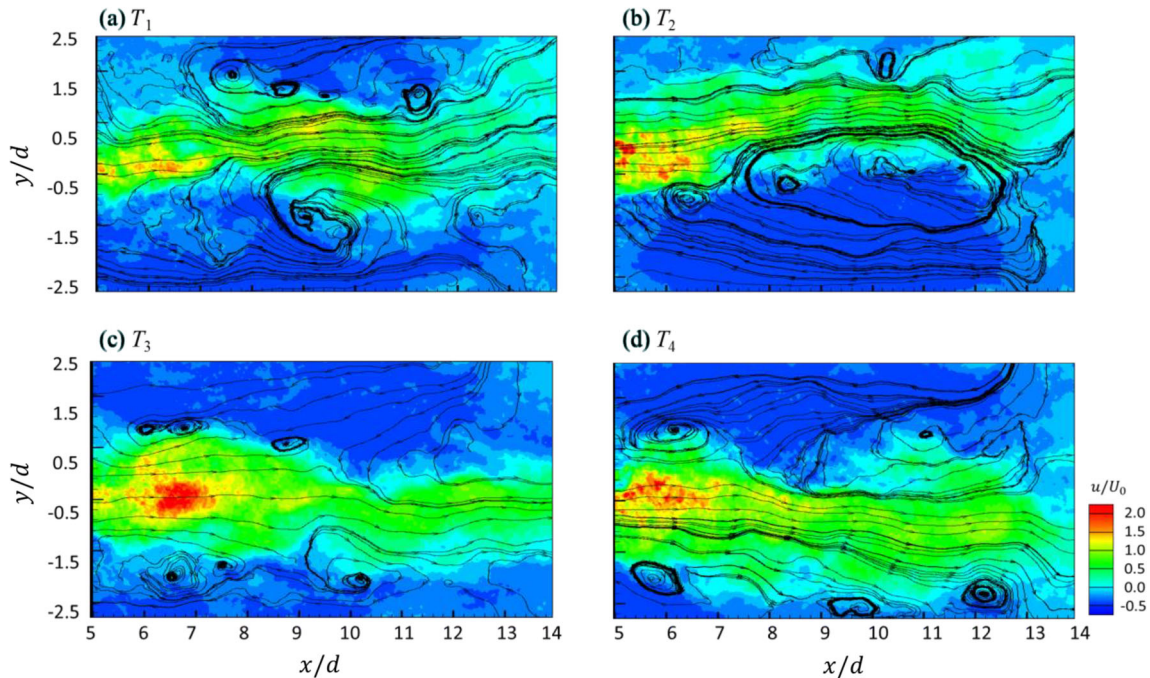**Fig.12** Temporal variation of the first POD mode coefficient in zone I
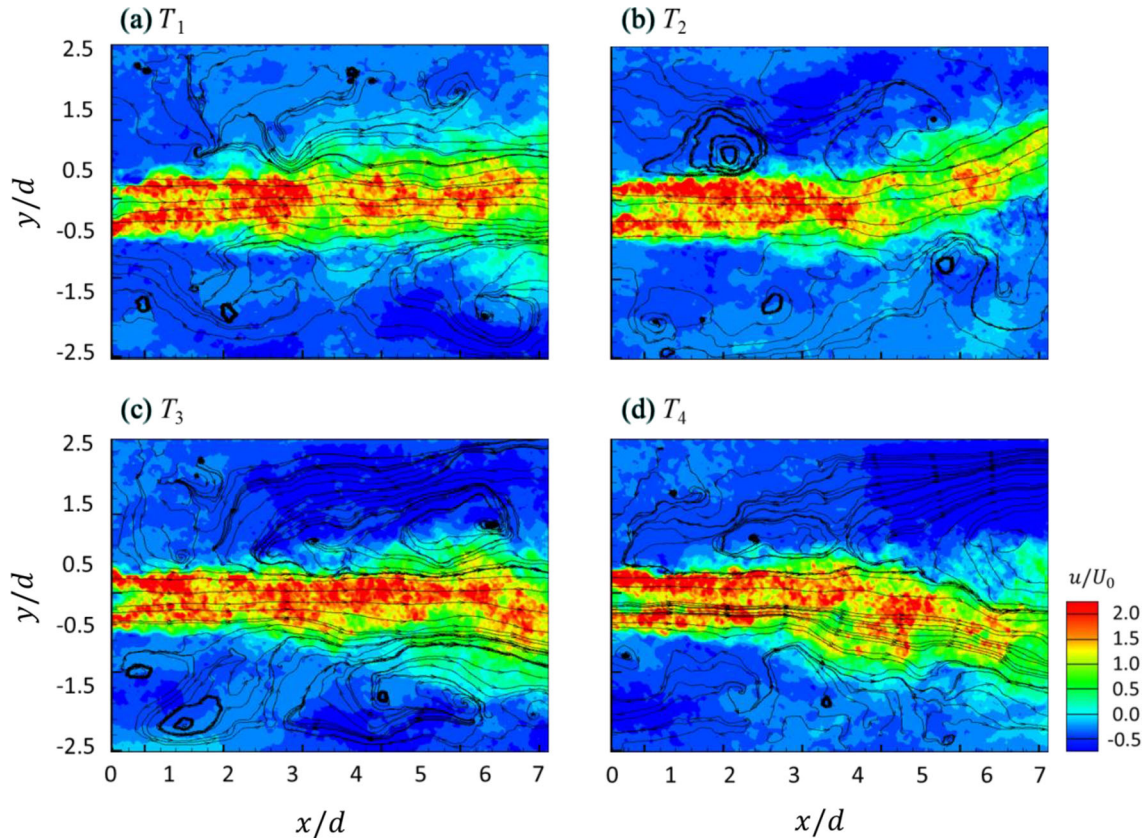
Fig.13 Reconstructed streamline pattern and contour plot of streamwise velocity field at four typical instants in zone I

and outer shear layers. In addition, vorticity was found in the boundary layer of the chamber wall and was caused by backflow and confinement. Subsequent correlative analysis indicated that coherent structures were mainly distributed in the shear layer and decayed with its development. The results also indicated that precession occurred in the region $x/d > 5$ and could lead to changes in the structure and position of the shear layer. Further spectral analysis indicated that a low-frequency structure with St $\approx 7.4 \times 10^{-3}$, which can be interpreted as precession, existed in the flow field and that the corresponding dominant frequency decreased as the fluid flowed downstream. In addition, POD analysis on the fluctuating velocity fields indicated that the most energetic POD mode represented the flow structures of precession in both zones, while other structures such as the AJ mode, smaller-scale structures in the shear layer and large-scale (flapping) oscillations of the inner jet were also identified. The precession induces alternating flow, out from one side of the chamber and in from the other side. Finally, low-order reconstruction, using the specified POD modes that captured 90% of the total energy, revealed the spatial distribution characteristics of large-

Fig.14 Temporal variation of the first POD mode coefficient in zone II

Fig.15 Reconstructed streamline pattern and contour plot of streamwise velocity field at four typical instants in zone II

scale coherent structures and the global variation of precession. The flow indicated that the mainstream oscillated up and down in zone I and twisted back and forth in zone II, with changes of the scale and position of flow structures on the measurement plane due to the instability of the reattachment point, thereby exposing complex behavior of the instantaneous flow field of precession.

References

Ball CG, Fellouah H, Pollard A (2012) The flow field in turbulent round free jets. Prog Aerosp Sci 50:1–26. https://doi.org/10.1016/j.paerosci.2011.10.002

Cafiero G, Ceglia G, Discetti S, Ianiro A, Astarita T, Cardone G (2014) On the three-dimensional precessing jet flow past a sudden expansion. Exp Fluids 55:1677

Ceglia G, Cafiero G, Astarita T (2017) Experimental investigation on the three-dimensional organization of the flow structures in precessing jets by tomographic PIV. Exp Thermal Fluid Sci 89:166–180. https://doi.org/10.1016/j.expthermflusci.2017.08.008

Chen X, Tian ZF, Kelso RM, Nathan GJ (2017) The topology of a precessing flow within a suddenly expanding axisymmetric chamber. J Fluids Eng 139(7):071201

Crow SC, Champagne F (1970) Orderly structure in jet turbulence. Boeing scientific research labs, Seattle, WA

Deane AE, Sirovich L (1991) A computational study of Rayleigh-Bénard convection. Part 1 Rayleigh-number scaling. J Fluid Mech 222:231–250

Fu H, He C, Liu Y (2020) Self-sustained oscillation of the flow in a double-cavity channel: a time-resolved PIV measurement. J Vis 23:245–257. https://doi.org/10.1007/s12650-020-00626-1

Graftieaux L, Michard M, Grosjean N (2001) Combining PIV, POD and vortex identification algorithms for the study of unsteady turbulent swirling flows. Meas Sci Technol 12:1422

He C, Liu Y (2017) Proper orthogonal decomposition of time-resolved LIF visualization: scalar mixing in a round jet. J Vis 20:789–815. https://doi.org/10.1007/s12650-017-0425-7

He C, Gan L, Liu Y (2019) The formation and evolution of turbulent swirling vortex rings generated by axial swirlers Flow. Turbul Combust 104:795–816. https://doi.org/10.1007/s10494-019-00076-2

Hill S, Nathan G (1995) Luxton R Precession in axisymmetric confined jets. In: proceedings of the twelfth australasian fluid mechanics conference. pp 135–138

Hutchinson P (1971) Stochastic tools in turbulence. IOP Publishing, Philadelphia

Kandakure MT, Patkar VC, Patwardhan AW (2008) Characteristics of turbulent confined jets. Chem Eng Process 47:1234–1245. https://doi.org/10.1016/j.cep.2007.03.012

Kiya M, Sasaki K (1983) Structure of a turbulent separation bubble. J Fluid Mech 137:83–113

Mi J, Nathan GJ (2004) Self-excited jet-precession Strouhal number and its influence on downstream mixing field. J Fluids Struct 19:851–862. https://doi.org/10.1016/j.jfluidstructs.2004.04.006

Mi J, Nathan GJ, Wong CY (2006) The influence of inlet flow condition on the frequency of self-excited jet precession. J Fluids Struct 22:129–133. https://doi.org/10.1016/j.jfluidstructs.2005.07.012

Nathan G (1988) The enhanced mixing burner (Doctoral dissertation)

Nathan G, Hill S, Luxton R (1998) An axisymmetric 'fluidic' nozzle to generate jet precession. J Fluid Mech 370:347–380

Newbold G (1998) Mixing and combustion in precessing jet flows. University of Adelaide, Adelaide

Newbold G, Nathan G, Nobes D, Turns S (2000) Measurement and prediction of NO_X emissions from unconfined propane flames from turbulent-jet, bluff-body, swirl and precessing jet burners. Proc Combust Inst 28:481–487

Newbold GJR, Nathan GJ, Luxton RE (2010) Large-scale dynamics of an unconfined precessing jet flame. Combust Sci Technol 126:71–95. https://doi.org/10.1080/00102209708935669

Nobes DS (1997) The generation of large-scale structures by jet precession. Thesis (Ph.D.) University of Adelaide, Dept. of Mechanical Engineering

Parham J, Nathan G, Hill S, Mullinger P (2005) A modified Thring-Newby scaling criterion for confined, rapidly spreading and unsteady jets. Combust Sci Technol 177:1421–1447

Semeraro O, Bellani G, Lundell F (2012) Analysis of time-resolved PIV measurements of a confined turbulent jet using POD and Koopman modes. Exp Fluids 53:1203–1220. https://doi.org/10.1007/s00348-012-1354-9

Sirovich L (1987a) Turbulence and the dynamics of coherent structures. I. Coherent Struct Q Appl Math 45:561–571

Sirovich L (1987b) Turbulence and the dynamics of coherent structures. II Symmetries and transformations. Q Appl Math 45:573–582

Sirovich L (1987c) Turbulence and the dynamics of coherent structures. III dynamics and scaling. Q Appl Math 45:583–590

Wang P, Ma H, Deng Y, Liu Y (2018) Influence of vortex-excited acoustic resonance on flow dynamics in channel with coaxial side-branches. Phys Fluids 30:095105. https://doi.org/10.1063/1.5049381

Wong CY, Lanspeary PV, Nathan GJ, Kelso RM, O'Doherty T (2003) Phase-averaged velocity in a fluidic precessing jet nozzle and in its near external field. Exp Thermal Fluid Sci 27:515–524. https://doi.org/10.1016/s0894-1777(02)00265-0

Wong C, Nathan G, Kelso R (2008) The naturally oscillating flow emerging from a fluidic precessing jet nozzle. J Fluid Mech 606:153–188

Yule A (1978) Large-scale structure in the mixing layer of a round jet. J Fluid Mech 89:413–432

Zaouali Y, Aissia HB, Jay J, Meslem A (2013) Experimental investigation of vortical structures in the near field of an axisymmetric jet by time-series analysis. Int J Fluid Mech Res 40(2):1–53

Zhang Q, Liu Y (2015) Influence of incident vortex street on separated flow around a finite blunt plate: PIV measurement and POD analysis. J Fluids Struct 55:463–483. https://doi.org/10.1016/j.jfluidstructs.2015.03.017